Femtosecond OPO pumped by a high power ytterbium rod-type fiber laser mode locked at harmonic repetition rates

Eric Freysz, Valerian Freysz

Femtosecond OPO pumped by a high power ytterbium rod-type fiber laser mode locked at harmonic repetition rates ⋆

FREYSZ Valerian[a], FREYSZ Eric[a,*]

[a] *Univ. Bordeaux, CNRS, LOMA UMR 5798, F-33400 Talence, France*

Abstract

We report on an optical parametric oscillator (OPO) pumped by femtosecond pulses delivered by a large-mode-area, ytterbium-doped, rod-type fiber laser. This femtosecond laser that is mode locked at harmonic repetition rates of 108 MHz, 216 MHz, and 324 MHz provides an average output power of more than 4.5 W and tens of nJ per pulse. The repetition rate is changed by adjusting the pulse polarization inside the laser cavity. Remarkably, at all these repetition rates and without any modification to the cavity, the OPO delivers femtosecond signal pulses that are tunable from 1450 nm to 1700 nm, with an average output power higher than 1 W. Increasing the pump power of the rod-type fiber and decreasing the transmission of the OPO output coupler, we were able to run the OPO at 540 MHz.

Keywords: Femtosecond pulse, Optical parametric oscillator, Tunable repetition rate laser, Rod-type fiber laser, Harmonic mode locking, ANDi laser, Ytterbium-doped fiber

⋆The authors acknowledge financial support from the French National Research Agency (ANR) in the frame of "the investments for the future" Programme IdEx Bordeaux – LAPHIA (ANR-10-IDEX-03-02) and the Conseil Région Nouvelle-Aquitaine

*Corresponding author

Email addresses: `valerian.freysz@u-bordeaux.fr` (FREYSZ Valerian), `eric.freysz@u-bordeaux.fr` (FREYSZ Eric)

1. Introduction

Given their interest in multiple, most notably in spectroscopy [1, 2], high-speed optical sampling [3, 4, 5], optical frequency comb [6, 7, 8], super-continuum generation [9], and others, high repetition rate (HRR) femtosecond lasers have attracted a lot of attention in the last decade. Many techniques have been used to design HRR lasers. For example, compact diode-pumped, mode-locked lasers with repetition rates of up to 101 GHz, which are able to generate 1.6 ps pulses in the 1.5 µm Telecom window have been demonstrated [10]. One can also generate picosecond pulses at an HRR using electro-optical modulation of a continuous wave laser [11]. In rare-earth-doped fiber, the HRR can be achieved by controlling the nonlinear polarization rotation in long and heavily doped erbium [12, 13] or ytterbium [14, 15] fibers. It has been demonstrated that the pulse repetition rate (PRR) can be adjusted by increasing the pump power or limiting the amplification bandwidth [16, 14, 15, 12]. At a given pump power, it has been further shown that PRR can be controlled by tuning the wave plates that set the polarization state of the pulses within the laser cavity. [12]. However, it is usually difficult to tune the central wavelength of oscillators by providing pulses at an HRR. In addition, the output power delivered by such an HRR oscillators is low and in the range of a few tens of milliwatts. Output powers of a few watts are usually achieved after two or three amplification stages. These power levels are required to further extend the domain of applications of HRR lasers and efficiently convert the central wavelength of the pulses into the ultraviolet (UV), visible, or infrared (IR) spectral ranges. Extension in the visible and UV spectral range is usually performed through second-harmonic generation (SHG) and sum-frequency generation (SFG) [17]. Further extension in the IR can be achieved through pumping an optical parametric oscillator (OPO) by amplifying the output of an HRR laser system [18, 19]. Compared with SHG and SFG, OPOs generate pulses that can be tuned on a broad spectral range, with limited pulse-to-pulse energy fluctuations and almost a TEM_{00} beam profile. In addition, the repetition rate of a synchronously pumped OPO can be

further increased using different means. The most common technique consists of dividing the cavity length L by an integer n or decreasing it by $(n-1)L/n$ [20]. This technique varies the amplitude of two successive pulses because the resonant pulse is transmitted numerous times by the output coupler in between each parametric amplification. An interesting way to avoid this problem while doubling the repetition rate is to pump the OPO in both forwards and backwards directions [21]. However this technique only doubles the PRR of an OPO. Hence, one of the simplest and efficient ways to generate tunable HRR femtosecond pulses on a broad spectral range is to pump an OPO with a high-power laser oscillator, where one can adjust the PRR. In the current paper, we perform an experiment using an ytterbium rod-type fiber that provides more than 4.5 W output power and tens of nJ per pulses, in which the PRR is controlled by nonlinear polarization rotation. At the three reported PRRs, the side mode suppression ratio (SMSR) is larger than 60 dB. The pulses delivered by this laser are further used to pump an OPO. Once optimized at a given repetition rate, the OPO is shown to work without any further adjustments. The femtosecond signal pulse delivered by this singly resonant OPO is tunable from 1450 nm to 1700 nm. Although the development and daily operation of this device requires a real expertise in laser physics, this source, which provides broadband and tunable pulses at an adjustable PRR, provides a way for increasing the research in scientific laboratories dealing with spectroscopy, photonic switching devices, all-optical sampling systems, high-bit rate optical communication systems, and other areas.

2. Experimental set-up

The entire experimental set-up is displayed in Fig. 1. The core of the set-up is a femtosecond high-power, self-mode-locked ytterbium rod-type fiber laser, which has been described elsewhere [22], and a linear and singly resonant OPO cavity built around a periodically polarized and MgO-doped lithium niobate crystal (MgO-PPLN). The duration of the pulses delivered by the laser and the OPO are measured using two homemade intensity autocorrelators. These

autocorrelators are based on a 3 mm BBO crystal cut for type I phase matching at 1030 nm and a Thorlabs Si photodiode FD11A coupled with a 10 MΩ transimpedance. The temporal resolution of the autocorrelator scanning optical delay line is ∼3 fs. The spectrum of the pulses yielded by the OPO and laser are measured using a Thorlabs Fourier-transform optical spectrum analyzers OSA205C. Finally, the pulse train and RF spectrum are acquired using a Hamamatsu pin diode head C1083-01 coupled with a Tektronix mixed domain oscilloscope MDO3102.

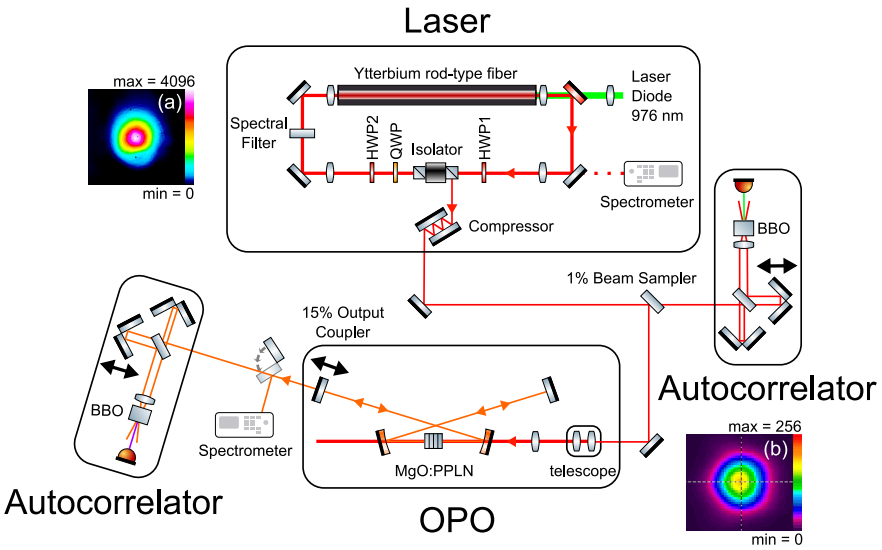

Figure 1: Set-up of the femtosecond large-mode-area fiber laser and the linear optical parametric oscillator. QWP, quarter-wave plate; HWP, half-wave plate; MgO:PPLN, Magnesium doped periodically polarized lithium niobate. a-b) spatial profile of the beam delivered by the laser and OPO, respectively.

2.1. The laser

The femtosecond pump laser is sketched in Fig. 1. The ring cavity is designed around a 0.75 m long large-mode-area (LMA) double-clad ytterbium rod-type fiber. It has a core diameter of 50 µm that results in a mode-field diameter of 50 µm at $\lambda = 1030$ nm and a pump-clad diameter of 170 µm. The nonlinear

coefficient of the fiber is estimated to be $\gamma \approx 2 \times 10^{-4}\,\mathrm{W^{-1}\,m^{-1}}$, and the absorption coefficient estimated at $\lambda \simeq 976\,\mathrm{nm}$ is $25\,\mathrm{dB\,m^{-1}}$. The fiber is cleaved and polished with an angle of 5°. A fiber-coupled laser diode emitting up to 55 W at $\lambda \simeq 974\,\mathrm{nm}$ is used to pump the laser. The diode beam transmitted through a dichroic mirror is focused on the pumping cladding of the LMA fiber. A 4 nm interference filter centered at $\lambda \simeq 1040\,\mathrm{nm}$ with transmission $> 90\,\%$ limits the spectral bandwidth of the laser. The latter is used to reduce the energy required for soliton generation, allowing for the pulsed mode regime. Finally, a nonlinear and partially transmitting mirror is built by combining a quarter-wave plate (QWP) and half-wave plates (HWP1, HWP2) with an optical isolator (OI), which takes advantage of nonlinear polarization evolution (NPE) within the LMA fiber [23]. The pulses yielded by the laser are sent through a pair of chirped mirrors (Layertech 110641) that compensate for the chirp induced by the propagation of the laser pulse in the amplifying fiber.

2.2. The OPO

The linear cavity of the OPO is sketched in Fig. 1. It is singly resonant for the signal pulse. The OPO is built around a 3 mm long MgO-PPLN (Covesion-MOPO1-1.0-3), in which five gratings with periods ranging from 29.52 µm to 31.59 µm are impinged. Both the input and output facets of the crystal are anti-reflection coated for the pump, signal, and idler waves (R<1.5 % at $\lambda \simeq 1064\,\mathrm{nm}$, $R < 1\,\%$ for λ in between 1400 nm and 1800 nm and R∼3 % - 2 % for λ in between 2600 nm and 4800 nm). The crystal is inserted in a thermally regulated oven whose temperature can be tuned to between 30 °C and 200 °C. Our linear OPO cavity is designed around two plane and two concave mirrors with a radius curvature of 10 cm (Layertec 131787). These have a transmission higher than 99 % at the pump wavelength and reflect more than 99 % at wavelengths in between 1.4 µm and 1.8 µm. In this spectral range, the transmission coefficient of the plane output coupler mirror is 85 % (Layertec 106828), whereas the other plane mirror is highly reflective (Layertec 131783). All the OPO mirrors have very low dispersion in the 1.4 µm to 1.8 µm spectral

range. The pump pulse is focused with a 20 cm focal length lens through the curved mirror in the MgO-PPLN. The cavity length for synchronous pumping at the 108 MHz first repetition rate of the fiber laser is ∼1.39 m. To compensate for the mismatch of the group velocity between the pump and the signal pulse within the PPLN, the output coupler is fixed on a high precision travel piezoelectric stage (SmarAct 300 mm SLLV42). The evolution of the phase-matching curves, the spectral bandwidth, and the group velocity mismatch between the pump and signal pulses of the OPO versus the temperature are presented in the supplementary material.

3. Results

3.1. The laser

First, we measured the pump laser threshold (∼6 W) without any wave-plates inserted into the system. We then increased the pump power up to 26 W, inserted the wave plates, and tuned their angles to improve the output power in the continuous wave regime. When optimized the output power delivered by the laser was ∼7.2 W. Its spectrum exhibited a narrow peak centered around 1.04 µm. From that point (as for a conventional ANDI laser), we set the angles of the HWP1, QWP, HWP2 to 114°, 86° and 276°, respectively, to ensure self-mode locking at the first PRR of $f_{rep} \simeq 108$ MHz. The output power was 4.5 W. For our ANDI laser, the self-mode-lock depended on three key parameters: the pump power, the bandwidth of the spectral filter, and the angle of the wave plates [24]. From a practical point of view, two points must be stressed. The first one is that, much like for all ANDI lasers using non polarizing fibers, the values of the angles of the wave plates will be different from one system to another. Second, around the self-mode locking, slight changes in the angle of the wave plates makes the laser work in an unstable Q-switched regime. For 26 W pump power, we were also able to reach 216 MHz and 324 MHz repetition rates. To adjust the PRR, we had to slightly rotate the QWP and HWP2 to make the laser operates in an unstable regime where harmonic repetition rates and multiple pulses would easily appear above a small continuous wave

background (CWB). In our set-up, this occurs setting the angle of the QWP and HWP2 at 105° and 298°, respectively. The output power delivered by the laser was then ∼7 W. By gently knocking on the table, we were able to randomly switch between the different PRRs. Upon knocking, the probability of achieving 216 MHz and 324 MHz PRR became ∼20 % and ∼5 %, respectively. Once set at a given PRR, we suppressed the CWB and further optimized the amplitude and pulse duration by adjusting the angle of the QWP and HWP2. The optimized positions of the wave plates were found to be 114° for the HWP1, 86°, 92° and 96° for the QWP and 276°, 298° and 298° for the HWP2 at 108 MHz, 216 MHz and 324 MHz PRR, respectively. The average output power increased with the PRR and was about 4.5 W, 5.5 W and 6.5 W at 108 MHz, 216 MHz and 324 MHz, respectively. The delivered pulse trains recorded by a fast photodiode are plotted in Fig. 2. The ringing of the response of the photodiode in the time domain was very likely because of the squared-off shape of its frequency response. The corresponding RF spectra, which is displayed in Fig. 3, shows the SMSR was > 60 dB for all the PRRs. At the same time, regardless of the PRR, the spatial profile displayed as an inset in Fig. 1 remained constant, with an $M^2 = 1.2 \pm 0.1$.

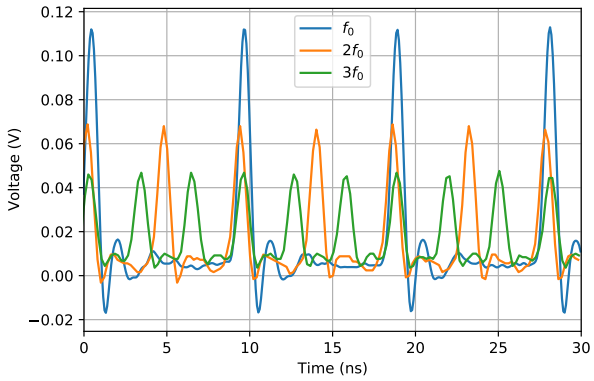

Figure 2: Pulse trains delivered by the femtosecond laser at the first f_0 (108 MHz [blue]), second $2f_0$ (216 MHz [orange]), and third $3f_0$ (324 MHz [green]) PRR. The energy per pulse decreases from 41.6 nJ to 20 nJ as the PRR increases from 108 MHz to 324 MHz.

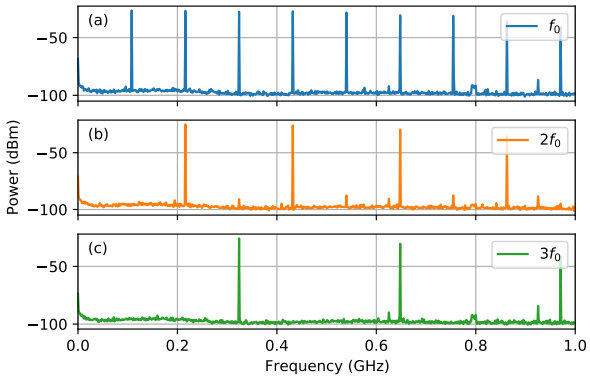

Figure 3: RF spectra of the laser pulses train at (a) first f_0 (108 MHz (blue)), (b) second $2f_0$ (216 MHz (orange)), and (c) third $3f_0$ (324 MHz (green)) PRR. The side mode suppression ratio is > 60 dB at all the frequencies.

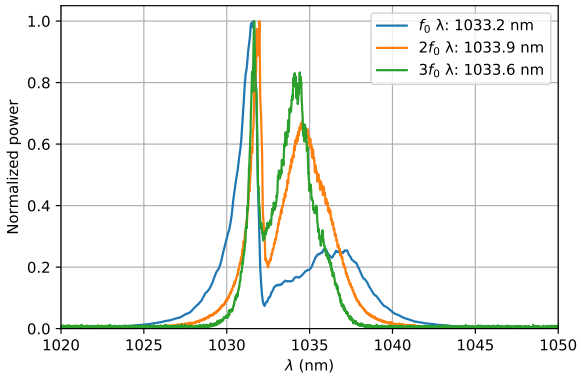

Figure 4: Spectra of the laser pulses at the first f_0 (108 MHz [blue]), second $2f_0$ (216 MHz[orange]), and third $3f_0$ (324 MHz [green]) PRR. For each spectrum, the normalization was performed by dividing the data by the maximum value. Here 95 % of the area under the spectra of the pulses at the first, second, and third PRR are about 13.2 nm, 9.1 nm and 7.8 nm, respectively. The values in the legend are the barycentric wavelengths.

We also recorded the evolution of the optical spectrum of the laser pulse at different PRRs (Fig. 4). The central wavelength remained almost constant and around 1033 nm, while the spectral width narrowed as the PRR increased as expected if looking at soliton theory [12]. About 95 % of the power was within 13.2 nm, 9.1 nm and 7.8 nm when the PRR was 108 MHz, 216 MHz and 324 MHz,

respectively.

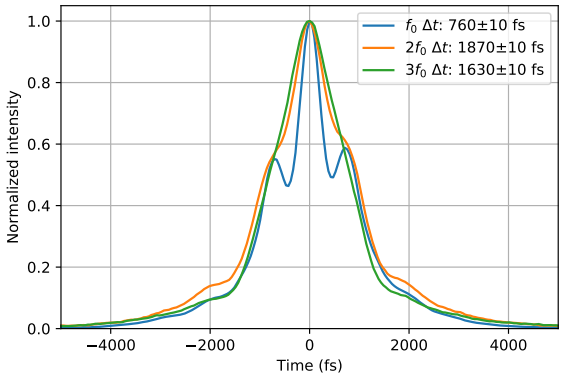

Figure 5: Autocorrelation traces of the chirped pulses delivered by the laser at the first f_0 (blue), the second $2f_0$ (orange), and the third $3f_0$ (green) PRR. For each autocorrelation trace, normalization was performed by dividing the data by the maximum value. The values in the legend are the temporal width at half the maximum value.

The duration of the chirped pulses delivered by the laser at the three different PRRs are plotted in Fig. 5. The autocorrelation duration at half the maximum value was found to be (1.75 ± 0.05) ps, (1.85 ± 0.05) ps and (1.60 ± 0.05) ps at 108 MHz, 216 MHz and 324 MHz, respectively. The autocorrelation traces of the laser pulses after six bounces on the chirped mirrors and their expected Fourier-transform limit as calculated from their spectra are presented in Fig. 6.

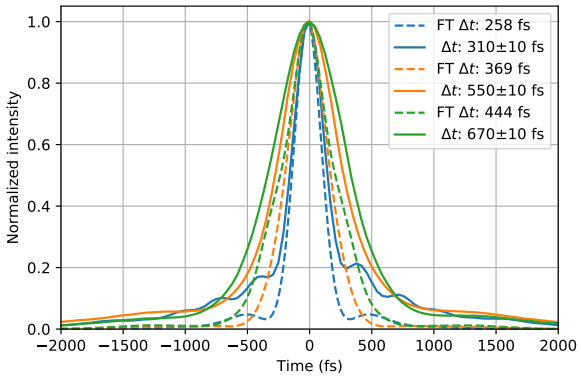

Figure 6: Autocorrelation traces of the chirped pulses delivered by the laser at the first f_0 (solid blue), the second $2f_0$ (solid orange), and the third $3f_0$ (solid green) PRR. The autocorrelation traces computed according to the recorded spectra are plotted with dashed lines. The values in the legend are the autocorrelation duration at FWHM. For each autocorrelation trace, normalization was performed by dividing the data by the maximum value.

The pulse durations were found to be (200 ± 10) fs, (360 ± 10) fs, and (440 ± 10) fs when considering a sech^2 pulse shape. The ratio R_A of the areas beneath the computed and experimental autocorrelation traces were 58.5 %, 72.6 % and 82.7 % for the 198 fs, 358 fs and 435 fs pulses, respectively. At its maximum, the pulse's energy E_{pump} decrease from 42 nJ, 25 nJ and 20 nJ as the PRR increases. The maximal peak powers P_{pump}^{peak} also decreased from 210 kW, 71 kW and 46 kW as the PRR increased. Hereafter, we will define the useful energy and useful peak power of the sech^2 pulse as $E_p = E_{pump} \times R_A$ and $P_p = P_{pump}^{peak} \times R_A$, respectively. The latter is associated with 123 kW, 53 kW and 38 kW for the 200 fs, 360 fs and 440 fs pulses. The FWHM pulse duration of the compressed pulse was larger than the optimal FWHM duration: the actual pulse duration was multiplied by a factor of 1.2, 1.5 and 1.5 at 108 MHz, 216 MHz and 324 MHz, respectively. Regarding the lesser pulses' recompression at the second and third harmonic PRR, it is worth mentioning the chirped mirror compressor was initially optimized at the first repetition rate. Although not reported here, the PRR of 540 MHz was also achieved by increasing the pump power by ∼8 %. The average output power, pulse duration, and peak power were then 7.0 W,

(810 ± 10) fs and 15.9 kW, respectively. A higher PRR can be achieved by further increasing the pump power. The main limit here is the thermal modal instability that may occur when LMA fibers are pumped above a given threshold [25]. Tables summarizing the determinations of all the parameters of the pump laser are presented in the supplementary material.

3.2. The OPO

The pulses delivered by the LMA rod-type ytterbium fiber laser were used to pump the OPO. First, we present the data recorded when the temperature of the MgO-PPLN reached 70 °C and when the 30.49 µm grating was used. At the pump wavelength ($\lambda \simeq 1034$ nm) and knowing the Sellmeier equations for the used lithium niobate crystal [26], phase matching was achieved for a pulse whose central wavelength was 1599 nm. The change in the output power produced by the OPO versus the pump power and for the different pump PRRs are presented in Fig. 7. The pump power was varied by using a $\lambda/2$ and a polarizing beam splitter in the pump beam's path.

Whatever the PRR, the average output power was more than 1 W and very stable (±1 %). The typical spatial profile of the pulse is depicted in inset (b) of Fig. 1, and its M^2 is ∼1.15. At a repetition rate of 108 MHz, the pump threshold of the OPO was found to be ∼0.5 W and the pump-to-signal slope efficiency ∼24.3 %. Unsurprisingly, as the PRR and pump pulse duration increased, the OPO pump threshold P_{pump}^{th} increased. It was approximately 1.71 W and 2.06 W at 216 MHz and 324 MHz PRR, respectively. Similarly, as the PRR increased, the pump-to-signal slope efficiency increased. It was approximately 29.3 % and 35.7 % at the second and third harmonic PRR, respectively.

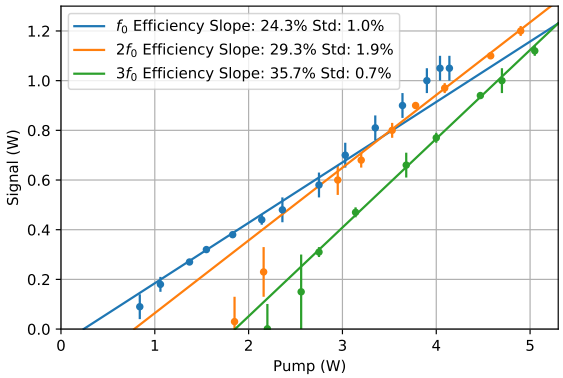

Figure 7: Evolution of the average output power delivered by the OPO versus the average pump power at the first f_0 (108 MHz (blue)), second $2f_0$ (216 MHz (orange)), and third $3f_0$ (324 MHz (green)) PRR using the 30.49 µm PPLN grating set at a temperature of 70 °C. The blue, orange, and green lines indicates the pump-to-signal slope efficiency. The standard deviations (Std) of the slope efficiency are indicated in the legend.

The increase of the OPO threshold versus the PRR was directly related to an increase of the pump pulse duration. Because in our experimental conditions we only changes the PRR, the parametric gain γ should only depend on the pump peak power. Taking into account the useful pump peak power at the threshold $P_p^{th} = P_{pump}^{th} \times R_A$, where P_{pump}^{th} is the pump peak power at threshold, P_p^{th} remained almost constant and was $\sim$ 15±1 kW at the OPO threshold. This indicates that most of the energy of the pump pulse not within the $sech^2$ pulse did not contribute to parametric amplification. Because R_A increased versus the PRR, the increase of the pump-to-signal slope efficiency versus the PRR was also likely related to the increase of the useful peak power P_p with the PRR.

The spectra of the signal pulses are presented in Fig. 8. As expected, no matter the pump PRR, the central wavelength remained almost constant. The width at half maximum of the spectrum narrowed when the pump pulse duration increased. It was 16.1 nm, 13.7 nm and 10.0 nm at 108 MHz, 216 MHz and 324 MHz, respectively, far below the 55.6 nm spectral acceptance of the 3 mm thick PPLN crystal.

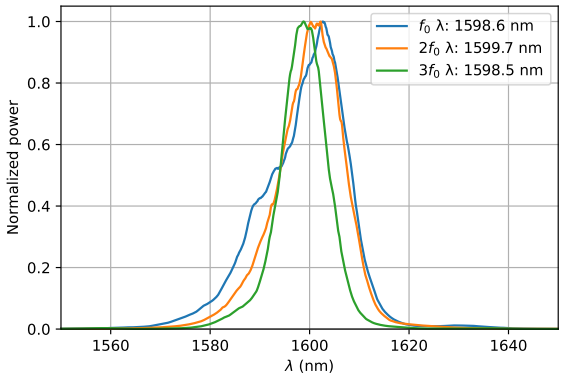

Figure 8: Spectra of the signal pulses delivered by OPO versus the pump PRR using the 30.49 µm PPLN grating set at a temperature of 70 °C at the first f_0 (108 MHz (blue)), second $2f_0$ (216 MHz (orange)), and third $3f_0$ (324 MHz (green)) PRR. The values in the legend are the barycentric wavelength. For each spectrum, normalization was performed by dividing the data by the maximum value.

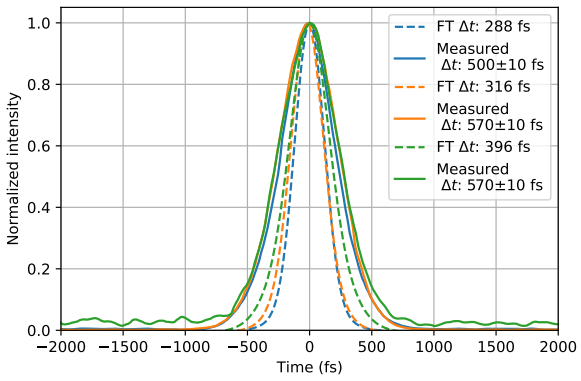

Figure 9: Evolution of the autocorrelation trace of the signal pulse delivered by the OPO using the 30.49 µm PPLN grating, where temperature was set at T= 70 °C at the first f_0 (108 MHz (blue)), second $2f_0$ (216 MHz (orange)), and third $3f_0$ (324 MHz (green)) PRR (full line). The autocorrelation Fourier-limited trace of the pulses computed according to the spectra are plotted with dashed lines. For each autocorrelation trace, normalization was performed by dividing the data by the maximum value.

Remarkably, the measured FWHM duration of the signal pulse, as presented in Fig. 9, only slightly increased versus the pump PRR. It was about (500 ± 10) fs, (570 ± 10) fs and (570 ± 10) fs at 108 MHz, 216 MHz and 324 MHz,

respectively. Considering the pulses were found to be Sech^2 in shape, the pulse duration was about (330 ± 10) fs, (370 ± 10) fs and (375 ± 10) fs. The spectral width of the generated wave supported a pulse duration at FWHM of about 290 fs, 315 fs and 395 fs. Therefore, the duration of the generated pulse was about 1.5 to 1.7 higher than their Fourier-transform limit. The latter pulse duration was measured at the maximum output power. At the expense of average power, we could get closer to the Fourier-transform limit by slightly shortening the cavity length [27].

By changing the temperature or the grating of the PPLN crystal, we change the central frequency of the signal pulse. We recorded the spectra and autocorrelation traces of the OPO pulses generated for the three different PRR at $\lambda \simeq 1470$ nm and $\lambda \simeq 1695$ nm. A summary of the spectra and autocorrelation width of these pulses at FWHM is presented in Tab. 1.

	108 MHz	**216 MHz**	**324 MHz**
		1470 nm	
Δt (fs)	290 ± 10	360 ± 10	420 ± 10
Δt FL (fs)	277	347	322
$\Delta\lambda$ (nm)	14.0 ± 0.5	13.0 ± 0.5	13.0 ± 0.5
		1695 nm	
Δt (fs)	490 ± 10	480 ± 10	500 ± 10
Δt FL (fs)	181	190	212
$\Delta\lambda$ (nm)	44.0 ± 0.5	24.0 ± 0.5	22.0 ± 0.5

Table 1: Summary of the measurements performed at $\lambda \simeq 1470$ nm and $\lambda \simeq 1695$ nm , respectively. Δt: Autocorrelation duration of the signal pulse at FWHM. $\Delta\lambda$ spectrum of the signal pulse at FWHM. Δt FL: Autocorrelation duration of the Fourier-limited signal pulse.

These pulses were generated using the 29.52 µm and 30.49 µm MgO-PPLN gratings, whose temperatures were set at $T = (40.0 \pm 0.1)$ °C and $T = (170.0 \pm 0.1)$ °C, respectively. At $\lambda \approx 1470$ nm, the FWHM pulse durations were (290 ± 10) fs, (360 ± 10) fs and (420 ± 10) fs at 108 MHz, 216 MHz and 324 MHz PRR, respectively. The generated pulses were almost Fourier-transform limited (∼1.2) at all the pump PRRs. At $\lambda \approx 1700$ nm, the FWHM pulse durations were

(490 ± 10) fs, (480 ± 10) fs and (500 ± 10) fs at 108 MHz, 216 MHz and 324 MHz PRR, respectively. They were two times larger than the Fourier-transform limit. This spectral broadening phenomenon was likely because of the larger group velocity mismatch between the pump and signal pulse at $\lambda \approx 1700$ nm.

We also pumped this OPO with the fifth harmonic PRR of our fiber laser (i.e. at 540 MHz). As already mentioned, at the maximum peak power of the pump, the pulses were about 16 kW, nearly at the $\sim 15 \pm 1$ kW peak pump threshold of our OPO. Hence, the OPO did not work when maintaining the 15 % output coupler. However, the OPO ran well using a 2 % output coupler.

4. Discussion and conclusion

The device presented above provides femtosecond pulses with more than 1 W of average power that are tunable on a broad spectral range at the harmonic repetition rate of a high-power ytterbium fiber laser. It is more complex than the continuum generation in fiber [28, 29] but yields a higher peak power at the given wavelengths. It also compared well with four waves mixing in the fiber, which has been shown to provide femtosecond pulses that are tunable on a smaller spectral range [30, 31, 32]. This system may offer some advantages if the user can reliably control the laser PRR. Indeed, the main drawback of the pump laser we developed is that the PRR switching is not well controlled. This limits its use in practical applications, unless this problem is properly addressed. In this regard, it should be mentioned that this issue has been tackled in more conventional fiber lasers by increasing the pump power and inserting passive fiber [33] or a Mach-Zehnder interferometer [34] into the laser.

In conclusion, we have reported on an LMA rod-type ytterbium-doped all-normal dispersion fiber laser that can yield more than 4.5 W output power and tens of nJ femtosecond pulses at up to 540 MHz. The control of the pulse repetition rate is based on nonlinear polarization rotation in a laser cavity . At all the pulse repetition rates, the SMSR were found to be larger than 60 dB. The compressed pulses delivered by this laser source are, without further amplification, used to pump an OPO. The singly resonant OPO was shown to work at

108 MHz, 216 MHz and 324 MHz without any change in the OPO cavity length. The femtosecond pulses delivered by this OPO were found to be tunable from 1400 nm to 1700 nm, and the average output power was higher than 1 W.

5. Bibliography

References

[1] A. Bartels, T. Dekorsy, H. Kurz, Femtosecond Ti:sapphire ring laser with a 2-GHz repetition rate and its application in time-resolved spectroscopy, Optics Letters 24 (14) (1999) 996–998, number: 14. doi:10.1364/OL.24.000996.

[2] R. Gebs, P. Klopp, G. Klatt, T. Dekorsy, U. Griebner, A. Bartels, Time-domain terahertz spectroscopy based on asynchronous optical sampling with femtosecond semiconductor disk laser, Electronics Letters 46 (1) (2010) 75, number: 1. doi:10.1049/el.2010.3062.
URL https://digital-library.theiet.org/content/journals/10.1049/el.2010.3062

[3] K. Weingarten, M. Rodwell, D. Bloom, Picosecond Optical Sampling of GaAs Integrated Circuits, IEEE Journal of Quantum Electronics 24 (2) (1988) 198–220, number: 2. doi:10.1109/3.115.

[4] S. Lecomte, L. Krainer, R. Paschotta, M. Dymott, K. Weingarten, U. Keller, Optical parametric oscillator with a 10-GHz repetition rate and 100-mW average output power in the spectral region near 1.5 m, Optics Letters 27 (19) (2002) 1714–1716, number: 19. doi:10.1364/OL.27.001714.

[5] J. B. Schlager, P. D. Hale, D. L. Franzen, High-sensitivity optical sampling using an erbium-doped fiber laser strobe, Microwave and Optical Technology Letters 6 (15) (1993) 835–837, number: 15 _eprint: https://onlinelibrary.wiley.com/doi/pdf/10.1002/mop.4650061503.
doi:https://doi.org/10.1002/mop.4650061503.
URL https://onlinelibrary.wiley.com/doi/abs/10.1002/mop.4650061503

[6] S. A. Diddams, The evolving optical frequency comb [Invited], JOSA B 27 (11) (2010) B51–B62, number: 11 Publisher: Optical Society of America. doi:10.1364/JOSAB.27.000B51.
URL https://www.osapublishing.org/josab/abstract.cfm?uri=josab-27-11-B51

[7] S. A. Diddams, L. Hollberg, V. Mbele, Molecular fingerprinting with the resolved modes of a femtosecond laser frequency comb, Nature 445 (7128) (2007) 627–630, number: 7128. doi:10.1038/nature05524.
URL http://www.nature.com/articles/nature05524

[8] M. E. Fermann, I. Hartl, Ultrafast Fiber Laser Technology, IEEE Journal of Selected Topics in Quantum Electronics 15 (1) (2009) 191–206, number: 1 Conference Name: IEEE Journal of Selected Topics in Quantum Electronics. doi:10.1109/JSTQE.2008.2010246.

[9] C. R. Head, H. Chan, J. S. Feehan, D. P. Shepherd, S. Alam, A. C. Tropper, J. H. V. Price, K. G. Wilcox, Supercontinuum Generation With GHz Repetition Rate Femtosecond-Pulse Fiber-Amplified VECSELs, IEEE Photonics Technology Letters 25 (5) (2013) 464–467, number: 5 Conference Name: IEEE Photonics Technology Letters. doi:10.1109/LPT.2013.2241420.

[10] A. E. H. Oehler, T. Südmeyer, K. J. Weingarten, U. Keller, 100 GHz passively mode-locked Er:Yb:glass laser at 1.5 µm with 1.6-ps pulses, Optics Express 16 (26) (2008) 21930–21935, publisher: Optical Society of America. doi:10.1364/OE.16.021930.
URL https://www.osapublishing.org/oe/abstract.cfm?uri=oe-16-26-21930

[11] A. Aubourg, J. Lhermite, S. Hocquet, E. Cormier, G. Santarelli, Generation of picosecond laser pulses at 1030 nm with gigahertz range continuously tunable repetition rate, Optics Letters 40 (23) (2015) 5610, number: 23. doi:10.1364/OL.40.005610.

URL https://www.osapublishing.org/abstract.cfm?URI=ol-40-23-5610

[12] Y. Ling, Q. Huang, Q. Song, Z. Yan, C. Mou, K. Zhou, L. Zhang, Intracavity birefringence-controlled GHz-tuning range passively harmonic mode-locked fiber laser based on NPR, Applied Optics 59 (22) (2020) 6724–6728, number: 22 Publisher: Optical Society of America. doi:10.1364/AO.398960.
URL https://www.osapublishing.org/ao/abstract.cfm?uri=ao-59-22-6724

[13] A. B. Grudinin, D. J. Richardson, D. N. Payne, Passive harmonic modelocking of a fibre soliton ring laser, Electronics Letters 29 (21) (1993) 1860–1861, number: 21 Conference Name: Electronics Letters. doi:10.1049/el:19931238.

[14] X. Zhu, C. Wang, S. Liu, G. Zhang, Tunable High-Order Harmonic Mode-Locking in Yb-Doped Fiber Laser With All-Normal Dispersion, IEEE Photonics Technology Letters 24 (9) (2012) 754–756, number: 9. doi:10.1109/LPT.2012.2188023.
URL http://ieeexplore.ieee.org/document/6178141/

[15] X. Zhu, C. Bu, C. Wang, R. Xu, G. Zhang, Harmonically Mode-Locked Twin-pulse Dissipative Solitons Yb-doped Fiber Laser, IEEE Photonics Technology Letters (2015) 4.

[16] A. Haboucha, A. Komarov, H. Leblond, F. Sanchez, G. Martel, Mechanism of multiple pulse formation in the normal dispersion regime of passively mode-locked fiber ring lasers, Optical Fiber Technology 14 (4) (2008) 262–267, number: 4. doi:10.1016/j.yofte.2008.01.001.
URL https://linkinghub.elsevier.com/retrieve/pii/S1068520008000023

[17] H. Ye, L. Pontagnier, C. Dixneuf, C. Dixneuf, G. Santarelli, E. Cormier, E. Cormier, Multi-GHz repetition rate, femtosecond deep ultraviolet

source in burst mode derived from an electro-optic comb, Optics Express 28 (25) (2020) 37209–37217, publisher: Optical Society of America. doi:10.1364/OE.409782.
URL http://www.osapublishing.org/oe/abstract.cfm?uri=oe-28-25-37209

[18] S. Lecomte, R. Paschotta, S. Pawlik, B. Schmidt, K. Furusawa, A. Malinowski, D. J. Richardson, U. Keller, Optical parametric oscillator with a pulse repetition rate of 39 GHz and 2.1-W signal average output power in the spectral region near 1.5 µm, Optics Letters 30 (3) (2005) 290–292, number: 3 Publisher: Optical Society of America. doi:10.1364/OL.30.000290.
URL https://www.osapublishing.org/ol/abstract.cfm?uri=ol-30-3-290

[19] S. Lecomte, R. Paschotta, S. Pawlik, B. Schmidt, K. Furusawa, A. Malinowski, D. Richardson, U. Keller, Synchronously pumped optical parametric oscillator with a repetition rate of 81.8 GHz, IEEE Photonics Technology Letters 17 (2) (2005) 483–485, number: 2. doi:10.1109/LPT.2004.839385.
URL http://ieeexplore.ieee.org/document/1386356/

[20] D. T. Reid, C. McGowan, W. Sleat, M. Ebrahimzadeh, W. Sibbett, Compact, efficient 344-MHz repetition-rate femtosecond optical parametric oscillator, Optics Letters 22 (8) (1997) 525–527, number: 8 Publisher: Optical Society of America. doi:10.1364/OL.22.000525.
URL https://www.osapublishing.org/ol/abstract.cfm?uri=ol-22-8-525

[21] J. Su, L. Chai, W. Liu, M. Hu, Mechanism and Implementation of a Bidirectional-Pumped Femtosecond Optical Parametric Oscillator With Single Cavity and Single Crystal, IEEE Journal of Quantum Electronics

55 (4) (2019) 1–5, number: 4. doi:10.1109/JQE.2019.2923437.
URL https://ieeexplore.ieee.org/document/8737981/

[22] P. Deslandes, M. Perrin, J. Saby, D. Sangla, F. Salin, E. Freysz, Picosecond to femtosecond pulses from high power self mode–locked ytterbium rod-type fiber laser, Optics Express 21 (9) (2013) 10731, number: 9. doi:10.1364/OE.21.010731.
URL https://www.osapublishing.org/oe/abstract.cfm?uri=oe-21-9-10731

[23] J. M. Dziedzic, R. H. Stolen, A. Ashkin, Optical Kerr effect in long fibers, Applied Optics 20 (8) (1981) 1403–1406, number: 8 Publisher: Optical Society of America. doi:10.1364/AO.20.001403.
URL https://www.osapublishing.org/ao/abstract.cfm?uri=ao-20-8-1403

[24] A. Chong, W. H. Renninger, F. W. Wise, Properties of normal-dispersion femtosecond fiber lasers, JOSA B 25 (2) (2008) 140–148, number: 2 Publisher: Optical Society of America. doi:10.1364/JOSAB.25.000140.
URL http://www.osapublishing.org/josab/abstract.cfm?uri=josab-25-2-140

[25] T. Eidam, C. Wirth, C. Jauregui, F. Stutzki, F. Jansen, H.-J. Otto, O. Schmidt, T. Schreiber, J. Limpert, A. Tünnermann, Experimental observations of the threshold-like onset of mode instabilities in high power fiber amplifiers, Optics Express 19 (14) (2011) 13218–13224, publisher: Optical Society of America. doi:10.1364/OE.19.013218.
URL http://www.osapublishing.org/oe/abstract.cfm?uri=oe-19-14-13218

[26] O. Gayer, Z. Sacks, E. Galun, A. Arie, Temperature and wavelength dependent refractive index equations for MgO-doped congruent and stoichiometric LiNbO3, Applied Physics B 91 (2) (2008) 343–348, number: 2.

doi:10.1007/s00340-008-2998-2.
URL http://link.springer.com/10.1007/s00340-008-2998-2

[27] A. Ryasnyanskiy, N. Dubreuil, P. Delaye, R. Frey, G. Roosen, Fourier transformed picosecond synchronously pumped optical parametric oscillator without spectral filtering element, Journal of the European Optical Society - Rapid publications 3 (0), number: 0 (Nov. 2008). doi:10.2971/jeos.2008.08037.
URL https://www.jeos.org/index.php/jeos_rp/article/view/08037

[28] H. L. Yu, X. L. Wang, P. Zhou, J. B. Chen, Multi-pulse operation of a dissipative soliton fibre laser based on nonlinear polarisation rotation, Quantum Electronics 46 (3) (2016) 213, number: 3 Publisher: IOP Publishing. doi:10.1070/QEL15927.
URL http://iopscience.iop.org/article/10.1070/QEL15927/meta

[29] Y. Wang, Y. Zhao, J. S. Nelson, Z. Chen, R. S. Windeler, Ultrahigh-resolution optical coherence tomography by broadband continuum generation from a photonic crystal fiber, Optics Letters 28 (3) (2003) 182. doi:10.1364/OL.28.000182.
URL https://www.osapublishing.org/abstract.cfm?URI=ol-28-3-182

[30] T. Gottschall, J. Limpert, A. Tünnermann, Ultra-short pulse fiber optical parametric oscillator, Optics Letters 42 (17) (2017) 3423. doi:10.1364/OL.42.003423.
URL https://www.osapublishing.org/abstract.cfm?URI=ol-42-17-3423

[31] T. Gottschall, T. Meyer, M. Schmitt, J. Popp, J. Limpert, A. Tünnermann, Four-wave-mixing-based optical parametric oscillator delivering energetic, tunable, chirped femtosecond pulses for non-linear biomedical applications, Optics Express 23 (18) (2015) 23968. doi:10.1364/OE.23.023968.

URL https://www.osapublishing.org/abstract.cfm?URI=oe-23-18-23968

[32] J.-C. Delagnes, R. Royon, J. Lhermite, G. Santarelli, H. Muñoz, T. Grosz, D. Darwich, R. Dauliat, R. Jamier, P. Roy, E. Cormier, High-power widely tunable ps source in the visible light based on four wave mixing in optimized photonic crystal fibers, Optics Express 26 (9) (2018) 11265. doi:10.1364/OE.26.011265.
URL https://www.osapublishing.org/abstract.cfm?URI=oe-26-9-11265

[33] S. Zhou, D. G. Ouzounov, F. W. Wise, Passive harmonic mode-locking of a soliton Yb fiber laser at repetition rates to 1.5 GHz, Optics Letters 31 (8) (2006) 1041–1043, number: 8 Publisher: Optical Society of America. doi:10.1364/OL.31.001041.
URL https://www.osapublishing.org/ol/abstract.cfm?uri=ol-31-8-1041

[34] R. Si Fodil, F. Amrani, C. Yang, A. Kellou, P. Grelu, Adjustable high-repetition-rate pulse trains in a passively-mode-locked fiber laser, Physical Review A 94 (1) (2016) 013813, number: 1 Publisher: American Physical Society. doi:10.1103/PhysRevA.94.013813.
URL https://link.aps.org/doi/10.1103/PhysRevA.94.013813